Multivalley Effective-Mass Approximation for Donor States in Silicon. I. Shallow-Level Group-V Impurities*

T. H. Ning† and C. T. Sah
Department of Physics and Materials Research Laboratory, University of Illinois at Urbana-Champaign, Urbana, Illinois 61801
(Received 12 July 1971)

Following the procedures of the Kohn-Luttinger one-valley effective-mass approximation (EMA), but without neglecting the intervalley overlap terms, a multivalley EMA is developed within the pseudopotential formalism for shallow-level group-V donors in silicon. A phenomenological two-parameter model impurity potential is proposed which behaves like a square well at small r and a screened Coulomb potential at large r. The relative smoothness of the model impurity potential compared with the true impurity potential justifies the use of the EMA. Within the EMA, the valley-orbit interaction can be incorporated completely in the energy calculations, instead of treated as a perturbation. The effects of the higher-energy subsidiary valleys and the $1s$-$2s$ coupling etc. can also be estimated quantitatively in this EMA. The energy levels of the group-V donor impurities in silicon are calculated using the variation method. The two potential parameters are adjusted to fit the observed $1s(A_1) \rightarrow 2p_\pm$ and $1s(T_2) \rightarrow 2p_\pm$ transition energies. It is shown that the proposed potential describes well the central-cell effects. For the p states, it is found that the usual one-valley approximation is adequate. It is also found that in the multivalley approximation the valley-orbit interaction shifts the $1s(A_1)$ level downward and the $1s(T_2)$ and $1s(E)$ levels upward relative to the one-valley $1s$ level. The effects of the uncertainty in the position of the Δ_1 conduction-band valleys and of the coupling between the $1s$ and $2s$ states on the ground-state energy are shown to be negligible. The contribution from wave-function components of an L_1 valley of the conduction band to the ground-state energy is computed to be less than 1% of that from wave-function components of a Δ_1 valley. It indicates that the higher-energy subsidiary conduction-band valleys may be neglected. The ground-state-model wave function is used to calculate the photo-ionization cross section and to predict the Fermi contact hyperfine constants. These results are compared with reported experimental and theoretical results.

I. INTRODUCTION

The Kohn-Luttinger[1-3] effective-mass approximation (EMA) has long been used to describe the electronic structure of shallow-level impurities in semiconductors. The impurity potential is assumed to be a simple Coulomb potential screened by the static dielectric constant. The agreement is excellent for the np energy levels for $n \geq 2$, but poor for the s states, especially the $1s$ state, because of central-cell effects.

In the case of shallow-level group-V donors in silicon, although Kohn and Luttinger[1-3] wrote the impurity wave function as a linear combination of the six wave functions each localized around one of the Δ_1 conduction-band minima, the overlap of these functions was completely neglected. This reduced the Schrödinger equation of the donor electron to six independent equations, one for each valley. Thus, the EMA of Kohn and Luttinger is essentially a one-valley EMA. It predicts a sixfold degeneracy (excluding spin degeneracy) of the s states, which, because of the tetrahedral symmetry of the substitutional impurity, are grouped into a singlet A_1, a doublet E, and a triplet T_2.[1,2] However, infrared absorption experiments by Aggarwal and Ramdas[4] showed that this degeneracy is lifted, with the $1s(A_1)$ forming the ground state and the $1s(E)$ lying slightly above the $1s(T_2)$. This splitting of the $1s$ level is attributed to the valley-orbit interaction.

The discrepancy between the Kohn-Luttinger one-valley theory and experiment for the shallow donor impurities in silicon is usually attributed to (i) the neglect of the central-cell correction to the impurity potential, (ii) the invalidity of screening by a dielectric constant in the vicinity of the impurity ion, (iii) the breakdown of the effective-mass approximation in the central-cell region, where the true impurity potential can no longer be assumed to be slowly varying, and (iv) the neglect of the intervalley overlap of the wave-function components in the calculation of the s-state energies.

Many attempts have been made to improve the agreement between the Kohn-Luttinger theory and experiment by taking into account one or more of these corrections,[5-11] or by improving the variational procedure used in the Kohn-Luttinger method.[12] Most of these attempts[5-7,9,10] aimed at accounting for the $1s(A_1)$ ground-state energy within the one-valley approximation; and one of the intrinsic difficulties of a theory in the one-valley approximation is its failure to account for the observed valley-orbit splitting of the s states. Fur-

thermore, as we shall demonstrate by our results, any central-cell-correction parameter obtained by fitting the ground-state energy in the one-valley approximation will undoubtedly overestimate the true effect of the correction considered.

It is evident that in order to calculate the valley-orbit splitting of the s states one must employ wave functions of the proper symmetry and must include all of the intervalley terms. By simply considering the symmetry of the A_1, T_2, and E states of the $1s$ level in the impurity core region, Kohn and Luttinger[1,2] were able to order correctly the relative energies of these states. However, since there is large variation of the observed valley-orbit interaction from one impurity to another,[4] it is clear that specific calculations will be required to account for the chemical trend.

Recently, Baldereschi[11] considered the simple Coulomb potential screened by a k-dependent dielectric function appropriate to the Δk values of the valley separation and treated the intervalley terms as a perturbation in Si and Ge. The estimated $1s(A_1)$-$1s(T_2)$ splitting was 10.6 meV, which is about $\frac{1}{3}$ of the $1s$ energy in the one-valley approximation. This result clearly demonstrates that the intervalley overlap of the donor impurity wave function must be taken into consideration in calculating the ground-state energy. Furthermore, since the splitting is comparable to the $1s$ energy in the one-valley approximation, it is desirable to derive a procedure which takes into consideration the intervalley terms completely rather than as a perturbation.

A one-band multivalley calculation of the $1s$-state energy of the group-V shallow donors (P, As, Sb) in silicon was first carried out by Morita and Nara.[8] By orthogonalizing the impurity wave function to the core states of the donor, their approach is in essence within the pseudopotential formalism. The EMA was used exterior to the impurity core region where a simple screened Coulomb potential was assumed, while within the impurity core region a first-principle true impurity potential was constructed from ionic potentials and a k-dependent dielectric function. The calculated $1s(E)$ and $1s(T_2)$ energies were satisfactory, but the calculated $1s(A_1)$ energies gave $E(\mathrm{P}) < E(\mathrm{As}) < E(\mathrm{Sb})$ for the three donor impurities, contrary to experimental results[4] which showed that $E(\mathrm{Sb}) < E(\mathrm{P}) < E(\mathrm{As})$. If one assumes that the one-band approximation is valid, then these results indicate that the first-principle impurity potential obtained by Morita and Nara is not sufficiently accurate.

In this paper we attempt to take into consideration all of the four corrections mentioned above. Corrections (iii) and (iv) are taken into consideration naturally by formulating the problem in the pseudopotential theory and in the multivalley effective-mass approximation, and we shall show that corrections (i) and (ii) can be described well by a phenomenological two-parameter model impurity potential.

The outline of this paper is as follows. In Sec. II, a phenomenological impurity potential is proposed and its physical significance discussed. In Sec. III, the multivalley EMA is developed and applied to calculate the energies of the s states, using the variation method and the proposed potential. In Sec. IV we discuss the potential parameters of the group-V impurities in terms of central-cell radii and ionic radii. In Sec. V, the validity of the various approximations made in the energy calculations is discussed; and in Sec. VI the impurity wave functions are used to predict the Fermi contact hyperfine constants, and to calculate the photo-ionization cross sections.

II. MODEL IMPURITY POTENTIAL

The true impurity potential U is a sum of terms which are invariant under the operations of the tetrahedral point group. The first few terms are given by[13]

$$U(\vec{\mathbf{r}}) = f(r) + g(r)xyz + h(r)\,(x^4 + y^4 + z^4 - \tfrac{3}{5}r^4) + \cdots \,. \tag{2.1}$$

The spherically symmetric term has the asymptotic values of

$$\lim_{r\to 0} f(r) = -\frac{e^2 \Delta Z}{r}\,, \quad \lim_{r\to\infty} f(r) = -\frac{e^2}{\epsilon r}\,, \tag{2.2}$$

where ΔZ is the difference between the atomic numbers of the donor and the silicon atoms, and ϵ is the static dielectric constant of silicon. The spherically symmetric part of U is by far the most important in determining the energy levels. The contribution of the anisotropic terms to the energies is expected to be small. In fact, since the s states have definite parities (see Sec. III), the expection value of $g(r)xyz$ is identically zero for the s states, so that the first anisotropic term has no effect on the s-state energies and splitting. Since it is difficult to estimate $g(r)$ and $h(r)$ even qualitatively, we shall not consider the anisotropic terms any further; and for the purpose of discussion we shall simply approximate U by $f(r)$.

Equation (2.2) gives the behavior of U at large values of r and as $r \to 0$. A qualitative behavior of U at intermediate values of r in the central-cell region may be obtained as follows. If we picture a Si^{+4} ion as a charge distribution, then the corresponding potential is

$$V(\mathrm{Si}^{+4}) = -\frac{Z_{\mathrm{Si}} e^2}{r} + e^2 \int d^3r' \frac{\sum_n |\psi_n(\vec{\mathbf{r}}')|^2}{|\vec{\mathbf{r}} - \vec{\mathbf{r}}'|}\,, \tag{2.3}$$

where Z_{Si} is the atomic number of silicon, and the sum is extended over all of the occupied orbitals

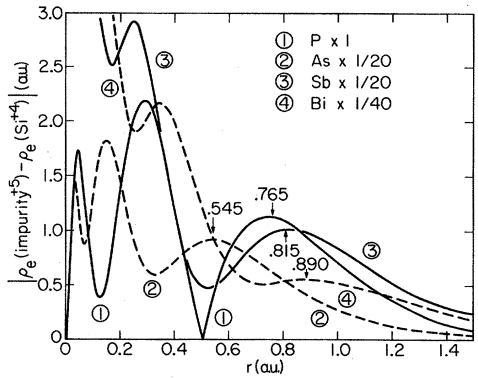

FIG. 1. Effective electronic radial charge densities of the group-V impurity ion cores in silicon. Arrows indicate the positions of the outermost peaks.

$(1s^2 2s^2 2p^6)$ of the Si^{+4} ion. Since all of the shells of the Si^{+4} ion are filled, the charge density $-e\sum_n |\psi_n|^2$ should be essentially spherically symmetric, so that (2.3) may be rewritten as

$$V(Si^{+4}) = -\frac{Z_{Si}e^2}{r} + e^2\int_0^r \frac{dr'}{r}\sum_n r'^2 R_n^2(r') + e^2\int_r^\infty \frac{dr'}{r'}\sum_n r'^2 R_n^2(r')$$

$$= -\frac{Z_{Si}e^2}{r} + e^2\int_0^r \frac{dr'}{r}\rho_e(Si^{+4}) + e^2\int_r^\infty \frac{dr'}{r'}\rho_e(Si^{+4}) , \quad (2.4)$$

where $R_n(r)$ is the radial part of $\psi_n(r)$, and

$$\rho_e(Si^{+4}) = \sum_n r^2 R_n^2(r) \quad (2.5)$$

is the radial electronic charge distribution function of the Si^{+4} ion. Similarly, the potential due to a group-V impurity ion I^{+5} is

$$V(I^{+5}) = -\frac{Z_I e^2}{r} + e^2\int_0^r \frac{dr'}{r}\rho_e(I^{+5}) + e^2\int_r^\infty \frac{dr'}{r'}\rho_e(I^{+5}) , \quad (2.6)$$

where $\rho_e(I^{+5})$ is the radial electronic charge distribution function of the I^{+5} ion. The bare impurity potential is

$$U_b(\vec{r}) = V(I^{+5}) - V(Si^{+4}) = -\frac{\Delta Z e^2}{r} + e^2\int_0^r \frac{dr'}{r}\Delta\rho_e(r') + e^2\int_r^\infty \frac{dr'}{r'}\Delta\rho_e(r') , \quad (2.7)$$

where $\Delta Z = [Z_I - Z_{Si}]$ is the difference between the atomic numbers of the impurity and the silicon atoms, and

$$\Delta\rho_e = [\rho_e(I^{+5}) - \rho_e(Si^{+4})] . \quad (2.8)$$

Inside the central-cell region, there is little dielectric screening by the valence electrons, so that the bare potential is approximately equal to the screened potential.

It should be noted that as defined by (2.3) and (2.6), the exchange energies have been neglected in $V(Si^{+4})$ and $V(I^{+5})$. We may partially take these exchange terms into account by using atomic core wave functions which are obtained with the exchange energies included. Using the Herman-Skillman table of atomic orbitals[14] we have computed $\Delta\rho_e$ of the group-V impurities. They are given in Fig. 1. The oscillations in $\Delta\rho_e$ imply that the potential U also oscillates in the central-cell region. This in turn implies that many Fourier components are needed to expand U.

The one-electron energy E and wave function ψ of the impurity problem are given by the wave equation

$$[H^0 + U]\psi = E\psi , \quad (2.9)$$

where H^0 is the one-electron Hamiltonian of the pure and perfect crystal. Since we are interested in the particular energies which lie between the conduction- and the valence-band edges, it is natural to expand ψ in terms of the Bloch functions ψ_{nk}^0 of the conduction and valence bands. In the case of a donor impurity in the one-band approximation, ψ is expanded in terms of the conduction-band Bloch functions ψ_k^0. By writing $\psi_k^0 = u_k e^{i\vec{k}\cdot\vec{r}}$, the periodic function $u_k^* u_{k'}$ can be expanded in the form

$$u_k^* u_{k'} = \sum_{\vec{G}} C(\vec{G}) e^{i\vec{G}\cdot\vec{r}} , \quad (2.10)$$

where $\vec{G}$ is a reciprocal-lattice vector. For silicon, u_k is made up of $3s$- and $3p_x$-like atomic orbitals,[15] so that many $\vec{G}$ components are required to expand $u_k^* u_{k'}$. Using (2.10) the matrix element of U may be written as

$$\langle\psi_k^0|\, U\,|\psi_{k'}^0\rangle = \sum_{\vec{G}} C(\vec{G})\, U(\vec{G}+\vec{k}'-\vec{k}) , \quad (2.11)$$

where $U(\vec{k})$ is the Fourier transform of $U(\vec{r})$. Now, as mentioned above, $U(\vec{G}+\vec{k})$ may not be negligible compared with $U(\vec{k})$, so that the usual effective-mass approximation,[1-3] which neglects $U(\vec{G}+\vec{k})$ for $\vec{G}\neq 0$, is no longer valid.

In this study, instead of giving up the EMA because of the strong and rapidly oscillating potential in the central-cell region, we introduce a phenomenological model impurity potential which averages out the oscillations and yet gives a good description of the central-cell effects. A more practical reason for using a phenomenological model potential is that the true potential cannot be determined from first principles with sufficient accuracy, as evidenced by the calculations of Morita and Nara.[8] Therefore, we propose to calculate the energies of the donor electron from the model wave equation

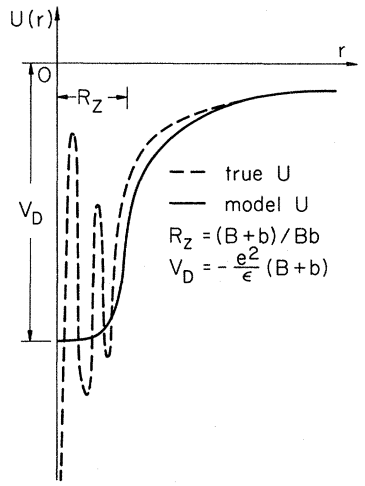

FIG. 2. Comparison of the proposed model impurity potential and the true impurity potential.

$$(H^0 + U)\Phi = E\Phi \,, \tag{2.12}$$

where the model potential is taken to be of the form

$$U(\vec{r}) = -(e^2/\epsilon r)\, Z_{\text{eff}}(r) = -(e^2/\epsilon r)(1 - e^{-br} + Bre^{-br}) \,, \tag{2.13}$$

and the model impurity wave function is expanded in the form

$$\Phi = \sum_{\vec{k}} F(\vec{k})\, \psi_k^0(\vec{r}) \,. \tag{2.14}$$

One of the advantages of working in the EMA is that the valley-orbit interaction may be easily included in the variation calculation of the energies. Also, in the EMA, some of the sources of discrepancy between theory and experiment can be examined easily (see Sec. V).

The proposed model impurity potential and the true impurity potential are shown schematically in Fig. 2 for comparison. The potential parameters b and B are adjusted to fit the variationally calculated $1s(A_1) \rightarrow 2p\pm$ and $1s(T_2) \rightarrow 2p\pm$ transition energies. At small r, the model potential looks like a spherical well, with a depth of $-e^2(B+b)/\epsilon$; and at large r, it behaves like a screened Coulomb potential. The turning point is given approximately by the position of maximum Z_{eff}, i.e., by $R_Z = (B+b)/Bb$. We shall further discuss the physical significance of R_Z in Sec. IV.

Since the model impurity potential differs from the true impurity potential only in the central-cell region, the corresponding model impurity wave function, which is given by (2.12) and (2.14), will differ from the true impurity wave function also only in the central-cell region. We shall make use of this property later in Sec. VI to calculate the Fermi contact hyperfine constants and the photoionization cross sections which depend on the impurity wave function only outside the central cell.

A further justification of using Eqs. (2.12) to (2.14) to describe the donor electron outside the central-cell region may be sought in the pseudopotential formalism. We have shown in the Appendix that in the pseudopotential formalism the pseudo-wave-equation of the donor electron may be written as

$$[H^0 + U_\phi]\Phi = E\Phi \,, \tag{2.15}$$

where H^0 is the one-electron Hamiltonian of the perfect crystal,

$$\Phi = \sum_{n\vec{k}} F_n(\vec{k})\, \psi_{n\vec{k}}^0 \tag{2.16}$$

is the pseudo-wave-function, U_ϕ is the pseudo-impurity-potential given by

$$U_\phi \Phi = (U + V_R)\Phi = U\Phi + \sum_{\alpha'} (E - E_{\alpha'}) \langle \psi_{\alpha'} | \Phi \rangle \psi_{\alpha'} \,, \tag{2.17}$$

and $\psi_{\alpha'}$ is a core-state wave function of the impure crystal.

As defined, V_R is a nonlocal repulsive potential which cancels part of U in the core regions. However, as shown in the Appendix, because Φ is expanded in the Bloch functions $\psi_{n\vec{k}}^0$, both the pseudo-wave-function and the pseudo-impurity-potential differ from the true wave function and the true impurity potential only in the core region of the impurity atom.

Many forms of pseudopotentials have been used in practice.[16,17] One convenient form of a phenomenological pseudopotential is the model potential V_M developed by Heine *et al.*[18,19] It represents the interaction of a conduction or valence electron with the ion core of an atom, and it has the form of

$$V_M = -\sum_l A_l P_l \quad \text{for } r < R_M$$
$$= -Ze^2/r \quad \text{for } r > R_M \,, \tag{2.18}$$

where P_l is the projection operator that picks out the component of the wave function with angular momentum l, and Z is the valency of the ion. Phillips[20] proposed that the pseudopotential form factor $V_\phi(\vec{q})$, including dielectric screening effects, for a homopolar covalent crystal has the form $V_\phi(\vec{q}) = V_M(\vec{q})/\epsilon(\vec{q})$, where $V_M(\vec{q})$ is the Fourier transform of $V_M(\vec{r})$ and $\epsilon(\vec{q})$ is the dielectric function of the crystal. This suggests that a possible form of the pseudo-impurity-potential is

$$U_M(\vec{r}) = \frac{1}{(2\pi)^3} \int d^3q \, \frac{\Delta V_M(\vec{q})}{\epsilon(\vec{q})}\, e^{i\vec{q}\cdot\vec{r}} \,, \tag{2.19}$$

where $V_M = [V_M(\text{impurity}) - V_M(\text{host})]$. Furthermore, since only the s states have appreciable amplitude in the core region and hence are affected by the short-range portion of the impurity potential, V_M can be approximated, for group-V impurities in Si, by

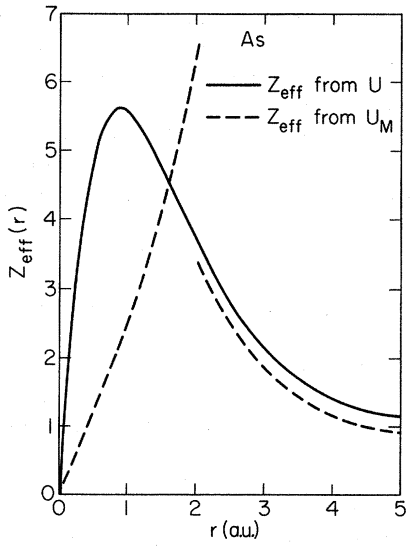

FIG. 3. Comparison of the effective charges of the proposed model impurity potential [Eq. (2.13)].and the so-called screened impurity model potential [Eq. (2.19)] for As in Si.

$$\begin{aligned}\Delta V_M &\simeq -\Delta A_0 \\ &= -[A_0(\text{impurity}) - A_0(\text{silicon})] \quad \text{for } r < R_M \\ &= -e^2/r \qquad\qquad\qquad\quad \text{for } r > R_M \ .\end{aligned} \tag{2.20}$$

Equation (2.19) gives the so-called screened impurity model potential used by Jaros.[9,21] As defined it has a discontinuity at $r = R_M$, which renders it unsuitable, if not unphysical, to be used in variation calculations. Furthermore, this potential does not give satisfactory results. When used in the one-valley approximation, as shown by Jaros,[9] the calculated energies are too small. However, when it is used in the multivalley approximation, we found that the calculated $1s(A_1)$-state energies are larger than the experimental ground-state energies by more than an order of magnitude.

The proposed model potential $U(\vec{r})$ given by (2.13) is continuous and has the same form as $U_M(\vec{r})$ given by (2.19).[22] This can best be demonstrated by plotting the effective charge Z_{eff} defined by $U(r) = -(e^2/\epsilon r)Z_{eff}(r)$. Z_{eff} for $U(\vec{r})$ and $U_M(\vec{r})$ are shown in Fig. 3 for As in Si, using A_0 given by Animalu and Heine[19] and $\epsilon(q)$ given by Nara and Morita.[23]

III. ENERGY LEVELS IN THE MULTIVALLEY EFFECTIVE-MASS APPROXIMATION

A. Variation Calculations and Results

As shown by Kohn and Luttinger,[1,2] because of the T_d symmetry of the point impurity in silicon crystal, the donor wave function decomposes according to the magnetic quantum number m of the envelope function into

$$\begin{aligned} m = 0: &\qquad A_1 + E + T_2 \ , \\ |m| \text{ even} (\neq 0): &\qquad A_1 + A_2 + 2E + T_1 + T_2 \ , \\ |m| \text{ odd}: &\qquad 2T_1 + 2T_2 \ . \end{aligned} \tag{3.1}$$

In the one-band approximation, the $1s$-state wave functions are given by

$$\Phi(\Gamma) = \sum_{i=1}^{6} \alpha_i(\Gamma) \sum_{\vec{k}} F_i(\vec{k}) \psi_k^0(\vec{r}) \ , \tag{3.2}$$

where

$$\alpha_i(A_1) = (1, 1, 1, 1, 1, 1)/\sqrt{6} \ , \tag{3.3}$$

$$\alpha_i(T_2) = \begin{cases} (1, -1, 0, 0, 0, 0)/\sqrt{2} \\ (0, 0, 1, -1, 0, 0)/\sqrt{2} \\ (0, 0, 0, 0, 1, -1)/\sqrt{2} \ , \end{cases} \tag{3.4}$$

and

$$\alpha_i(E) = \begin{cases} \tfrac{1}{2}(1, 1, -1, -1, 0, 0) \\ \tfrac{1}{2}(1, 1, 0, 0, -1, -1) \ . \end{cases} \tag{3.5}$$

The envelope function $F_i(\vec{k})$ is localized around the ith of the six Δ_1 conduction-band minima. Following the procedure for the one-valley EMA[1,2] we define the Fourier transform as

$$F_i(\vec{r}) = (1/\sqrt{V}) \sum_{\vec{k}} F_i(\vec{k}) \exp[i(\vec{k} - \vec{k}_i) \cdot \vec{r}] \ , \tag{3.6}$$

where $\vec{k}_i$ is the position of the ith conduction-band minimum, and V is the volume of the crystal. The envelope functions $F_i(\vec{r})$ are taken as trial functions in the variation calculations, and they are assumed to have the same form as in the one-valley EMA.[1,2] For example, $F_5(\vec{r})$ is taken to be

$$F_5(\vec{r}) = [1/(\pi a_t^2 a_l)^{1/2}] \exp\{-[(x^2 + y^2)/a_t^2 + z^2/a_l^2]^{1/2}\} \ , \tag{3.7}$$

where a_t and a_l are variational parameters, which may be thought of as the effective Bohr radii of the $1s$ state.

It can be shown from group-theoretic arguments[24] that if the impurity potential is assumed to have tetrahedral symmetry, then there is no mixing of the $\Phi(\Gamma)$'s belonging to different representations. Therefore, the $1s$-state energies are given by (2.12) and (3.2) as

$$E(\Gamma) = \frac{\langle \Phi(\Gamma) | H^0 + U | \Phi(\Gamma) \rangle}{\langle \Phi(\Gamma) | \Phi(\Gamma) \rangle} \ , \tag{3.8}$$

where Γ can be A_1, T_2, or E.

In principle, Eq. (3.8) gives the energy $E(\Gamma)$ in terms of the variational parameters a_t and a_l. However, the evaluation of $\langle \Phi | \Phi \rangle$ and $\langle \Phi | U | \Phi \rangle$ using (3.7) is time consuming since it involves complicated three-dimensional integrals. Furthermore, because of the intervalley terms, the kinetic-energy term $\langle \Phi | H^0 | \Phi \rangle$ is very complicated

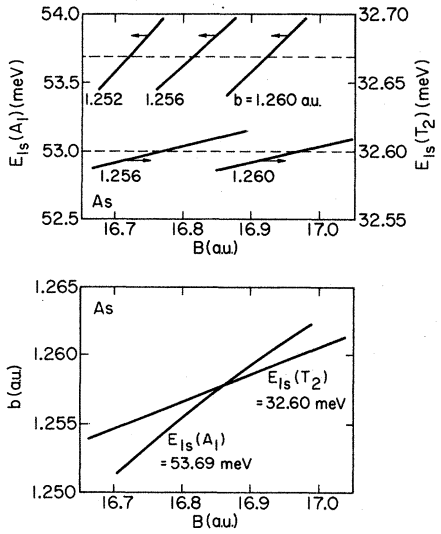

FIG. 4. $1s(A_1)$- and $1s(T_2)$-state energies of As in Si as a function of the potential parameters.

to evaluate if (3.7) is used. Therefore, an alternative simplification procedure is adopted using the multivalley spherical-band approximation: (i) $F_i(\vec{r})$ is hydrogenic, so that $a_t = a_l = a$ in Eq. (3.7), and (ii) $E_k^0 = E_c + \hbar^2(\vec{k} - \vec{k}_i)^2/2m^*$ for $\vec{k}$ near $\vec{k}_i$.

We use the value of $m^* = 0.29819m_0$ which gives the same one-valley $1s$ energy of 30.879 meV as the one-valley ellipsoidal-band case of $m_l = 0.9163m_0$ and $m_t = 0.1905m_0$[25] for the impurity potential $-e^2/\epsilon r$. We found that this value of m^* holds for $11.41 \leq \epsilon \leq 11.70$.

Using the spherical-band approximation, the kinetic-energy term $\langle \Phi | H^0 | \Phi \rangle$, the potential-energy term $\langle \Phi | U | \Phi \rangle$, and the normalization term $\langle \Phi | \Phi \rangle$ can all be reduced to closed forms in terms of the variational parameter a. For the $1s$ states, these terms are

$$\langle \Phi | H^0 | \Phi \rangle = \sum_{i,j} \alpha_i(\Gamma)\alpha_j(\Gamma) \frac{\hbar^2}{2m^*} \frac{8}{a^2} \left(\frac{a^2|\vec{k}_i - \vec{k}_j|^2 + 2}{[4 + a^2|\vec{k}_i - \vec{k}_j|^2]^2} \right), \tag{3.9}$$

$$\langle \Phi | U | \Phi \rangle = \sum_{i,j} \alpha_i(\Gamma)\alpha_j(\Gamma) \left(-\frac{4e^2}{\epsilon a} \right) \times \left(\frac{1}{[4 + a^2|\vec{k}_i - \vec{k}_j|^2]} - \frac{1}{[(2+ab)^2 + a^2|\vec{k}_i - \vec{k}_j|^2]} + \frac{2aB(2+ab)}{[(2+ab)^2 + a^2|\vec{k}_i - \vec{k}_j|^2]^2} \right), \tag{3.10}$$

and

$$\langle \Phi | \Phi \rangle = \sum_{i,j} \alpha_i(\Gamma)\alpha_j(\Gamma) \frac{16}{[4 + a^2|\vec{k}_i - \vec{k}_j|^2]^2} . \tag{3.11}$$

The energies are determined by minimizing $E(\Gamma)$ with respect to a. We use $\epsilon(59\,^\circ\mathrm{K}) = 11.46$ for the static dielectric constant of Si, which is deduced from the room-temperature index of refraction $n = 3.417$,[26] and the temperature coefficient $(1/n)(dn/dT) = (3.9 \pm 0.4) \times 10^{-5}\ (^\circ\mathrm{C})^{-1}$.[27] The parameters b and B are adjusted to fit the experimental $1s(A_1) \rightarrow 2p_\pm$ and $1s(T_2) \rightarrow 2p_\pm$ transition energies. The position of the Δ_1 conduction-band minima is assumed to be at $k_i = 0.85k_{\max}$. The effects of k_i are analyzed in Sec. V. The resulting dependence of the $1s(A_1)$ and $1s(T_2)$ energies on the potential parameters is illustrated for As in Fig. 4.

For the s states, the intervalley overlap contributes a factor of order $1/(1 + a^2k_i^2)^2$ to the normalization constant $\langle \Phi | \Phi \rangle$. For the group-V impurities this amounts to about 10^{-4}, so that the intervalley overlap of the wave function is indeed negligible. However, the probability density $\Phi^*\Phi$ near $r = 0$ is maximum for the A_1 state but zero for the T_2 and E states due to symmetry. This, together with the fact that the model impurity potential is large near $r = 0$, is responsible for the splitting of the s states.

Using the appropriate trial envelope functions, the same procedures can be applied to evaluate the energies of the $2s$, $2p_0$, and $2p_\pm$ states, etc. For the $2p_0(T_2)$ state [$m = 0$ in Eq. (3.1)] we found that the intervalley contribution to the energy is small as expected, and is less than 0.04% in all cases for the potential parameters used. This indicates that for p states the usual one-valley approximation should be adequate. In the one-valley approximation, there is no need to make the spherical-band approximation because variation calculations can be carried out in the parabolic-band approximation. Hence, for the $2p$ and $3p$ states the energies are calculated using the one-valley parabolic-band EMA.

The results of the variation calculations for the group-V impurities in silicon, together with available experimental optical data are given in Table I, where the experimental data have been adjusted so that the $2p_\pm$ levels are the same as the theoretical value (6.33 meV).

The small discrepancies between theory and experiment for the s states are partly due to using the spherical-band approximation, and to the neglect of phonon broadening and shift at the finite temperature of the experiments. Some other possible sources of discrepancy will be discussed in Sec. V.

B. Valley-Orbit Interaction

The intervalley coupling has the effect of lifting the sixfold degeneracy of the s states predicted by the one-valley EMA. The energy shifts can be obtained by comparing the multivalley EMA energies with the one-valley EMA energy. In Table II the $1s$ variational energies in the one-valley

approximation using the same potential and parameters as in the multivalley approximation are given. By comparing with the results of Table I, we see that for all of the group-V impurities the valley-orbit interaction shifts the $1s(A_1)$ level downward and the $1s(T_2)$ and $1s(E)$ levels upward relative to the $1s$ level in the one-valley approximation. These shifts are illustrated schematically in Fig. 5.

TABLE I. Binding energies of the group-V donors in Si.

	State	Variation parameters (a.u.) a_t	a_l	Energy (E_c-E) (meV) Theory[a]	Experiment
	$3p_\pm$	50.5	31.0	2.811	3.06(4.2 °K)[b]
	$2p_\pm$	50.5	31.0	6.326	6.33(4.2 °K)[b]
	$2s(E)$	37.1	37.1	7.895	···
	$2s(T_2)$	36.2	36.2	8.042	···
P	$2s(A_1)$	31.4	31.4	8.947	···
	$2p_0$	34.0	20.5	11.352	11.39(4.2 °K)[b]
	$1s(E)$	35.6	35.6	32.376	32.37(59 °K)[c]
	$1s(T_2)$	33.7	33.7	33.740	33.74(59 °K)[c]
	$1s(A_1)$	23.1	23.1	45.469	45.47(4.2 °K)[c]
	$3p_\pm$	50.5	31.0	2.811	3.08(4.2 °K)[b]
	$2p_\pm$	50.5	31.0	6.326	6.33(4.2 °K)[b]
	$2s(E)$	37.8	37.8	7.790	···
	$2s(T_2)$	37.0	37.0	7.921	9.03(4.2 °K)[d]
As	$2s(A_1)$	29.7	29.7	9.257	···
	$2p_0$	34.0	20.5	11.352	11.45(4.2 °K)[b]
	$1s(E)$	37.1	37.1	31.458	31.19(59 °K)[c]
	$1s(T_2)$	35.4	35.4	32.601	32.60(59 °K)[c]
	$1s(A_1)$	18.4	18.4	53.690	53.69(4.2 K)[c]
	$3p_\pm$	50.5	31.0	2.811	2.99(4.2 °K)[b]
	$2p_\pm$	50.5	31.0	6.326	6.33(4.2 °K)[b]
	$2s(E)$	37.6	37.6	7.824	···
	$2s(T_2)$	36.8	36.8	7.945	···
Sb	$2s(A_1)$	32.3	32.3	8.786	···
	$2p_0$	34.0	20.5	11.352	11.39(4.2 °K)[b]
	$1s(E)$	36.6	36.6	31.753	30.40(59 °K)[c]
	$1s(T_2)$	35.1	35.1	32.818	32.82(50 °K)[c]
	$1s(A_1)$	25.0	25.0	42.680	42.68(4.2 °K)[c]
	$3p_\pm$	50.5	31.0	2.811	3.05(4.2 °K)[e]
	$2p_\pm$	50.5	31.0	6.326	6.33(4.2 °K)[e]
	$2s(E)$	38.0	38.0	7.757	···
	$2s(T_2)$	37.3	37.3	7.872	8.71(4.2 °K)[f]
Bi	$2s(A_1)$	27.9	27.9	9.624	···
	$2p_0$	34.0	20.5	11.352	11.34(4.2 °K)[e]
	$1s(E)$	37.6	37.6	31.182	···
	$1s(T_2)$	36.1	36.1	32.161	32.16[g]
	$1s(A_1)$	14.0	14.0	70.901	70.90(4.2 °K)[e]

[a]The potential parameters b and B used are given in Table II.

[b]See Ref. 33.

[c]See Ref. 4.

[d]See Ref. 31.

[e]See Ref. 28.

[f]See Ref. 32.

[g]See Ref. 29. The $1s(T_2)$ level of Bi in Si is spin-orbit split, with the $[1s(A_1)-\text{quartet}]=39.08$ meV and $[1s(A_1)-\text{doublet}]=38.08$ meV. Here we have assumed that the $1s(T_2)$ level before spin-orbit splitting (see Ref. 30) has an energy given by $[1s(T_2)-1s(A_1)]=[(\text{doublet})+(\frac{2}{3})(\text{quartet}-\text{doublet})]$, i.e., $[1s(T_2)-1s(A_2)]=38.74$ meV.

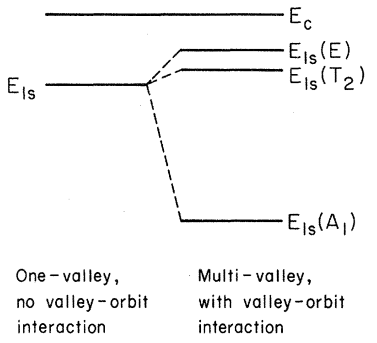

FIG. 5. Schematical illustration of the valley-orbit splitting of the $1s$ levels.

Table I shows that the degeneracy of the $2s$ states is also lifted, the $2s(E)$-$2s(A_1)$ splitting being 1.05, 1.47, 0.96, and 1.87 meV for P, As, Sb, and Bi, respectively. These compare well with the estimates of $2s(E)$-$2s(A_1)=1.3$, 1.6, and 0.4 meV for P, As, and Sb, respectively, previously obtained by Kohn and Luttinger[1] who assumed the $2s(T_2)$ and $2s(E)$ states to be degenerate.

The results of Tables I and II show that the central-cell correction gives a shift of only about 4 meV to the ground-state energy if the one-valley approximation is used, while a shift of 12–40 meV is obtained in the multivalley approximation. Thus, it is evident that the use of parametric central-cell correction to fit the one-valley EMA ground-state energy to experiment, without properly taking into account the valley-orbit interaction, will overestimate the true effect of the correction considered.

IV. CHEMICAL TREND OF CENTRAL-CELL RADIUS AND IONIC RADIUS

As discussed earlier, in Sec. II, the proposed model impurity potential [Eq. (2.13)] looks like a

TABLE II. The $1s$ state energy in the one-valley spherical-band approximation, $m^*=0.29819m_0$.

	Potential parameters (a.u.) b	B	Variation parameter (a.u.) a	Energy (E_c-E) (meV)
P	0.8724	7.310	32.7	34.498
As	1.2577	16.861	33.6	33.789
Sb	1.0118	8.648	34.0	33.548
Bi	1.589	31.92	33.7	33.715
Coulomb	∞	0.0	38.4	30.879

TABLE III. Comparison of R_Z with R_{ion}.

	b (a.u.)	B (a.u.)	R_Z (a.u.)	R_{ion} (a.u.)	R_Z/R_{ion}
P	0.8724	7.310	1.283	0.765	1.68
As	1.2577	16.861	0.8544	0.545	1.57
Sb	1.0118	8.648	1.104	0.815	1.35
Bi	1.589	31.92	0.6607	0.630	1.05

spherical well at small r, and it behaves like a screened Coulomb potential at large r. The boundary is given approximately by the position of maximum Z_{eff}, $R_Z=(B+b)/Bb$. Qualitatively, R_Z represents the radius beyong which the central-cell correction to the impurity potential is unimportant. Therefore, we expect R_Z to be correlated somehow with the radius R_{ion} of the effective charge distribution of the impurity ion core.

R_{ion} may be estimated as follows. In Sec. II, we found that the true impurity potential in the central-cell region is given qualitatively by a point charge of $e\Delta Z$ at the nucleus plus an effective electronic radial charge density of $-e\Delta\rho_e(r)$ [Eqs. (2.7) and (2.8)]. R_{ion} should be given by some weighted average of the peak positions of $|\Delta\rho_e|$. However, we shall adopt the simplest definition, namely R_{ion} = position of the outermost maximum of $|\Delta\rho_e|$. Examination of Fig. 1 shows that this definition works well for the group-V impurities, except for Bi. In the case of Bi, the outermost maximum of $|\Delta\rho_e|$, which occurs at 0.890 a.u., is so weak that it certainly overestimates R_{ion}(Bi). The effective value of R_{ion}(Bi) should lie somewhere between the outermost and the second outermost peaks of $|\Delta\rho_e|$. We shall assume that R_{ion}(Bi) = 0.630 a.u., which is midway between the outermost and the second outermost peaks. In Table III we compare R_Z and R_{ion} of the group-V donors. The comparison shows that R_Z is larger than R_{ion} by about 5–70%. Also, the ratio R_Z/R_{ion} decreases as the atomic number increases. As we shall see immediately below, this chemical trend is completely consistent with the comparison between ion radius and radius of maximum radial charge density of the ion in crystals.

Slater[34] observed that Pauling's ionic radii[35] are consistently larger than the radii of maximum radial charge density in the outermost shell of electrons in the corresponding ions, by a ratio of about 1.5–3.0 for the monovalent and divalent ions. Furthermore, for the ions which belong to the same group in the Periodic Table, this ratio decreases as the atomic number of the ion increases. This observation suggests that we make a similar comparison for the group-V ions.

In Table IV, we compare Pauling's ionic radius[35] of a group-V ion with the radius of maximum radial charge density in the outermost shell of electrons in the ion core. The latter is taken from Table II of Waber and Cromer,[36] which actually gives the core orbital of the neutral atoms rather than of the ions. (The Herman-Skillman orbitals[14] from which we obtained R_{ion} are also orbitals of the neutral atoms.) The results show that the ionic radius is larger than the radius of the core charge distribution by a ratio of about 1.35–1.85. Also, this ratio decreases as we go through the sequence from P to Bi.

Comparing Tables III and IV, we see that the values of R_Z are indeed consistent with the concept of an effective radius of the impurity ion core. Furthermore, the good quantitative agreement substantiates the interpretation that R_Z measures the effective core radius of the impurity ion, beyond which the central-cell correction to the impurity potential is unimportant.

The existence of R_{ion} for P indicates that although both Si and P have the same core configuration, the charge distribution in the two cores are quite different. It also accounts for the large R_Z for P while it has the smallest ion core of the four impurities.

V. SOME POSSIBLE SOURCES OF DISCREPANCY

A. Effects of the Uncertainty in k_i

In Sec. III, we assumed that the Δ_1 conduction-band minima are located at a distance of $k_i = 0.85k_{max}$ from the center of the Brillouin zone. Actually, experimental results by the ENDOR method[37–39] indicate that $k_i/k_{max}=0.85\pm0.03$. This uncertainty in k_i/k_{max} does not affect the calculated p-state energies because there the intervalley terms are all negligible. However, variations in k_i/k_{max} would change the calculated valley-orbit splitting which in the multivalley approximation is a function of the intervalley separation.

In Table V we give a comparison of the quantities of interest as a function of k_i/k_{max} for the case of Sb in Si. It is seen that the effect of the uncertainty in k_i/k_{max} on these quantities is small.

B. Coupling between the 1s and the 2s States

It can be shown by group-theoretical arguments[24]

TABLE IV. Comparison of Pauling's ionic radii with the radii of maximum charge density in the outermost shell of electrons in the ions.

Ion	Ionic radius (Å)	Shell radius of core (Å)	Ratio
P^{+5}	0.34	0.184 (2p)	1.85
As^{+5}	0.47	0.274 (3p)	1.71
Sb^{+5}	0.62	0.440 (4d)	1.41
Bi^{+5}	0.74	0.542 (5d)	1.37

that the matrix element of the donor electron Hamiltonian H between states $\Phi_1(\Gamma)$ and $\Phi_2(\Gamma)$ of the same representation does not in general vanish. Hence the $1s(A_1)$ state could be coupled to the $2s(A_1)$, the $2p_0(A_1)$, and the $3d_0(A_1)$ states, etc. Similarly, the $1s(E)$ and the $1s(T_2)$ states could be coupled to the higher-E and higher-T_2 states, respectively.

In Sec. III we assumed that the energy could be calculated by the variation method from expressions like

$$E_{1s}(\Gamma)=\frac{\langle\Phi_{1s}(\Gamma)|H|\Phi_{1s}(\Gamma)\rangle}{\langle\Phi_{1s}(\Gamma)|\Phi_{1s}(\Gamma)\rangle} \tag{5.1}$$

and

$$E_{2s}(\Gamma)=\frac{\langle\Phi_{2s}(\Gamma)|H|\Phi_{2s}(\Gamma)\rangle}{\langle\Phi_{2s}(\Gamma)|\Phi_{2s}(\Gamma)\rangle} \ . \tag{5.2}$$

This is equivalent to neglecting the coupling between a given symmetry state and other states of the same symmetry. In this section we examine the effect of such coupling on the energies calculated.

In the case of the one-valley EMA, Faulkner[12] considered the first 9 s-like and the first 18 p-like energy levels and found that for silicon there is negligible energy shift due to the interaction among the levels.

In the multivalley approximation we shall assume that the $1s$ state is coupled appreciably only to the $2s$ state. Coupling between the $1s$ and $3s$ states may be neglected because of the larger energy separation. Thus, the $1s$ and the $2s$ energy levels are given by the secular equation

$$\begin{vmatrix} \langle\Phi_{1s}|H|\Phi_{1s}\rangle - E\langle\Phi_{1s}|\Phi_{1s}\rangle & \langle\Phi_{1s}|H|\Phi_{2s}\rangle \\ \langle\Phi_{2s}|H|\Phi_{1s}\rangle & \langle\Phi_{2s}|H|\Phi_{2s}\rangle - E\langle\Phi_{2s}|\Phi_{2s}\rangle \end{vmatrix} = 0 \ . \tag{5.3}$$

As a specific example, we consider phosphorus. Using the same $k_i/k_{\max}$ and potential parameters as in Table I, the individual terms can be evaluated in terms of the variational parameter a. The energies are then determined by minimizing $E_{1s}(\Gamma)$ and $E_{2s}(\Gamma)$ with respect to a. The results are given in Table VI, where we have also listed from Table I the corresponding energies with no coupling. The $1s(A_1)$ level is shifted most, but it amounts to only 1.8%.

We expect the effects of the $1s$-$2s$ coupling to be even smaller for the deeper impurities because of the larger energy separations.

C. Contribution to the Ground-State Energy from the Higher Subsidiary Conduction-Band Minima

Band-structure calculations for silicon[40,41] indicate that there are subsidiary valleys or saddle points of higher energy at L_1, K_1, and U_1, etc., points of the lowest conduction band besides the six Δ_1 minima. However, thus far, in the multivalley approximation we have included only the six Δ_1 valleys, and the contribution to both the wave function and the energy from the higher symmetry points have been neglected. To introduce wave-function components from all of these subsidiary valleys into the variation calculations would make the problem prohibitively complicated and would require a more accurate picture of the band structure than is presently available. Nevertheless, the contribution to the ground-state energy from a higher subsidiary valley, say at L_1, can be compared with that from a Δ_1 valley as follows.

Consider a Δ_1 valley at $(0.85,\ 0,\ 0)k_{\max}$ and a L_1 valley at $(0.5,\ 0.5,\ 0.5)k_{\max}$. The total wave function is

$$\Phi = C_{\Delta_1}|\Delta_1\rangle + C_{L_1}|L_1\rangle \ , \tag{5.4}$$

where $|\Delta_1\rangle$ and $|L_1\rangle$ are the wave functions for the Δ_1 valley and the L_1 valley in the one-valley approximation. The mixing-in of the L_1-valley component has the effect of lowering the Δ_1-valley energy by

$$\delta E_{\Delta_1\text{-}L_1}=\frac{|\langle\Delta_1|H|L_1\rangle|^2}{\langle L_1|H|L_1\rangle-\langle\Delta_1|H|\Delta_1\rangle} \ . \tag{5.5}$$

The matrix elements $\langle\Delta_1|H|\Delta_1\rangle$ and $\langle L_1|H|L_1\rangle$ are just the one-valley energies of the Δ_1 valley and the L_1 valley, respectively. If we assume that the effective masses for the two valleys are not much different, then we may write[40]

$$\langle L_1|H|L_1\rangle-\langle\Delta_1|H|\Delta_1\rangle \simeq \text{energy separation between } \Delta_1 \text{ valley and } L_1 \text{ valley} \simeq 0.7 \text{ eV} \ . \tag{5.6}$$

TABLE V. Comparison of the potential parameters b and B, the variation parameter a, the energy levels, and the peak position R_Z of the effective impurity charge as a function of $k_i/k_{\max}$ for Sb in Si.

$k_i/k_{\max}$	Potential parameters[a] (a.u.) b	B	R_Z (a.u.)	State	Variation parameter a (a.u.)	Energy (meV) Theory
				$1s(E)$	36.6	31.761
0.88	1.0409	9.320	1.068	$1s(T_2)$	35.1	32.820
				$1s(A_1)$	24.8	42.680
				$1s(E)$	36.6	31.753
0.85	1.0118	8.648	1.104	$1s(T_2)$	35.1	32.818
				$1s(A_1)$	25.0	42.680
				$1s(E)$	36.6	31.748
0.82	0.9817	7.995	1.144	$1s(T_2)$	35.1	32.818
				$1s(A_1)$	25.2	42.680

[a] b and B are determined by fitting the theoretical $1s(A_1)\rightarrow 2p_\pm$ and $1s(T_2)\rightarrow 2p_\pm$ energies to the experimental values.

TABLE VI. The effect of coupling between the $1s$ and $2s$ states on the energy levels of P in Si.

State	Energy (meV) No coupling	With coupling	Shift
$2s(E)$	7.895	7.895	<0.001
$2s(T_2)$	8.042	8.042	<0.001
$2s(A_1)$	8.947	8.926	−0.021
$1s(E)$	32.376	32.390	0.014
$1s(T_2)$	33.740	33.780	0.040
$1s(A_1)$	45.469	46.298	0.829

The matrix element $\langle \Delta_1 | H | L_1 \rangle$ is then just an intervalley matrix element of H.

Assuming that the parameters in Table I hold for both the Δ_1 and the L_1 valleys, we have calculated the energy shifts for the group-V impurities. They are given in Table VII. The energy shift is small in all cases compared with the one-valley energy of the Δ_1 valley, which is about 34 meV, indicating that the L_1 component is negligible.

Recently, Castner[42] and Castner *et al.*[43] considered the mixing into the Δ_1 components the L_1, K_1, and U_1 components and obtained shifts which are about 10 times our estimates. They assumed the mixing interaction to be the impurity potential and the shifts in energy were calculated from expressions of the form

$$\frac{|\langle \Delta_1 | U | L_1 \rangle|^2}{\langle L_1 | H | L_1 \rangle - \langle \Delta_1 | H | \Delta_1 \rangle} .$$

By neglecting the kinetic energy term $|\langle \Delta_1 | H^0 | L_1 \rangle|^2$, which we found to be of the same order of magnitude as the potential energy term $|\langle \Delta_1 | U | L_1 \rangle|^2$, they probably overestimated the contributions from the L_1, K_1, and U_1 components.

VI. APPLICATIONS

A. Photo-Ionization Cross-Section

The photo-ionization cross section $\sigma_I(\hbar\omega)$ of a donor electron from its ground state is given by[44]

$$\sigma_I(\hbar\omega) = \left[\left(\frac{E_{\text{eff}}}{E_0}\right)^2 \frac{n}{\epsilon}\right] \frac{4\pi^2\alpha}{3} \hbar\omega \sum_f |\langle f | \vec{r} | 1s(A_1) \rangle|^2 \times \delta(E_f + E_I - \hbar\omega) , \quad (6.1)$$

where n is the optical index of refraction, ϵ is the optical dielectric constant, E_{eff}/E_0 is the effective electric-field ratio at the trap center, $\alpha = e^2/\hbar c$ is the fine structure constant, $|1s(A_1)\rangle$ is the ground state of the donor electron, and $|f\rangle$ is the final state in the continuum. Now, the appropriate unit of distance in the impurity problem is the effective Bohr radius a of the ground state. Therefore, most of the contribution to the dipole matrix element $\langle f | \vec{r} | 1s(A_1) \rangle$ comes from wave-function components at distances larger than a from the donor nucleus. At such distances it is justified to use the model impurity wave function for $|1s(A_1)\rangle$ and plane waves for $|f\rangle$. With these approximations, we obtain

$$\sigma_I(\hbar\omega) = \left[\left(\frac{E_{\text{eff}}}{E_0}\right)^2 \frac{n}{\epsilon}\right] \frac{4\pi\alpha}{3} a^2 S(\hbar\omega) , \quad (6.2)$$

where $S(\hbar\omega)$ is a dimensionless shape function given by

$$S(\hbar\omega) = 256 \left(\frac{2m^*}{\hbar^2}\right) \hbar\omega a^5 \frac{[(2m^*/\hbar^2)(\hbar\omega - E_I)]^{3/2}}{[1 + a^2(2m^*/\hbar^2)(\hbar\omega - E_I)]^6} . \quad (6.3)$$

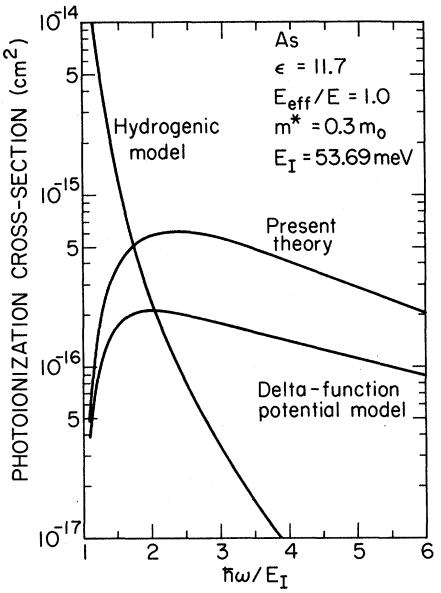

FIG. 6. Photo-ionization cross sections of As in Si.

In Fig. 6, the photo-ionization cross section for As is plotted and compared with the cross sections given by the scaled hydrogenic model[44] and by Lucovsky's δ-function potential model.[45] The spectral dependence of the present model and the δ-function potential model are similar. The cross sections rise from zero at $\hbar\omega = E_I$, reach a maximum, and then fall off. This is to be contrasted with the hydrogenic model which has a maximum at $\hbar\omega = E_I$. Most of the experimental photo-ioniza-

TABLE VII. Energy shifts due to the introduction of the L_1 components into the Δ_1 components.

	Energy shift (meV)
P	0.037
As	0.089
Sb	0.021
Bi	0.17

tion cross sections of shallow impurities in silicon reported are for acceptors.[46,47] However, the photoconductive response observed by Onton[48] for silicon doped with antimony or phosphorus shows spectral dependence similar to that predicted by the present model or by the δ-function potential model.

B. Fermi Contact Constants

The Fermi contact hyperfine constant a_l, which measures the coupling between the spin of the donor electron and the spins of the Si^{29} nuclei neighboring the donor, is given by[37]

$$a_l = \frac{16\pi}{3}\,\frac{\mu_{Si}}{I_{Si}}\,\mu_e\,|\psi(\vec{r}_l)|^2\,, \tag{6.4}$$

where $|\psi(\vec{r}_l)|^2$ is the probability density of the ground-state electron at the lth silicon site, μ_e is the magnetic moment of the electron, μ_{Si} and I_{Si} are the magnetic moment and spin, respectively, of the Si^{29} nucleus. Outside the impurity core region, it is justified to approximate the true wave function by the model wave function. Therefore, in terms of the envelope functions, we have[38,49]

$$|\psi(\vec{r}_l)|^2 \simeq |\Phi(\vec{r}_l)|^2$$

$$= \tfrac{2}{3}\eta\,|F(\vec{r}_l)|^2\,[\cos k_i x_l + \cos k_i y_l + \cos k_i z_l]^2\,, \tag{6.5}$$

where

$$\eta = \frac{|\psi^0_{k_i}(\vec{r}_l)|^2}{\langle \psi^{0\,2}_{k_i}\rangle_{\text{av over unit cell}}} = 178 \pm 18\,, \tag{6.6}$$

$$F(\vec{r}) = e^{-r/a}/(\pi a^3)^{1/2}\,, \tag{6.7}$$

and ψ^0_k is the Bloch function of the conduction band. In Sec. III we found that $a(P) = 23.1$ a.u., $a(\text{As}) = 18.4$ a.u., and $a(\text{Sb}) = 25.0$ a.u. Using $k_i/k_{\max}$ as a parameter to match the experimental values of the Fermi contact constants for the lattice sites identified definitely or tentatively by Castner,[42] we obtained a mean value of $k_i/k_{\max} = 0.856$. This is in good agreement with the values $k_i/k_{\max} = 0.87 \pm 0.01$ reported by Castner,[42] and $k_i/k_{\max} = 0.85 \pm 0.03$ reported by Feher.[38] It is also consistent with the value of $k_i/k_{\max} = 0.85$ used in the energy calculations.

Using $k_i/k_{\max} = 0.856$ in Eqs. (6.4) and (6.5), the calculated values of the Fermi contact constants are given in Table VIII, where the arrangement of the experimental values is due to Castner.[42] Also shown in Table VIII are the theoretical results by Castner,[42] who included the wave-function components from the regions of the L_1, K_1, and U_1 points of the lowest conduction band into the ground-state wave function, and the results by Hale and Mieher. However, as discussed in Sec. V, we found that Castner's analysis probably overestimated the contribution from these higher-energy symmetry

TABLE VIII. The Fermi contact hyperfine constants in units of Mc/sec.

Site	Donor	Theory $a_l/2$ TGC[b]	Theory $a_l/2$ HM[c]	Theory $a_l/2$ Present[d]	Experiment[a] $a_l/2$	Experiment[a] Shell	Experiment[a] Shell identified
	As	4.032	5.201	6.035	3.860		
(0, 0, 4)	P	3.316	4.184	3.827	2.981	*A*	√
	Sb	3.399	3.684	3.230	3.101		
	As	0.611	0.927	0.898	0.758		
(0, 0, 8)	P	0.560	0.851	0.714	0.663	*K*	√
	Sb	0.485	0.794	0.645	N. F.[e]		
	As	0.667	1.051	0.750	0.642		
(1, 1, 1)	P	0.444	0.733	0.418	0.270	*E*	√
	Sb	0.308	0.604	0.340	0.293		
	As	0.356	1.485	2.237	···		
$(\bar{3}, \bar{3}, \bar{3})$	P	0.379	1.271	1.518	···		
	Sb	0.492	1.149	1.308	···		
	As	0.643	0.917	1.337	0.801		
(4, 4, 4)	P	0.644	0.839	1.001	0.689	*H*	
	Sb	0.746	0.780	0.888	0.703		
	As	1.746	1.089	1.770	2.037		
(5, 5, 5)	P	1.458	1.055	1.462	1.649	*C*	√
	Sb	1.236	1.004	1.335	1.397		
	As	0.475	0.557	0.823	0.739		
$(\bar{7}, \bar{7}, \bar{7})$	P	0.505	0.595	0.827	0.598	O	
	Sb	0.571	0.590	0.801	0.670		
	As	0.411	···	0.028	0.694		
(8, 8, 8)	P	0.253	···	0.032	0.739	*J*	
	Sb	0.173	···	0.031	N. F.		
	As	0.524	···	0.250	0.607		
(9, 9, 9)	P	0.487	···	0.306	0.612	*N*	
	Sb	0.433	···	0.314	N. F.		
	As	1.165	0.578	0.779	1.121		
(2, 2, 0)	P	0.803	0.450	0.462	0.840	*F*	√
	Sb	0.722	0.389	0.383	0.504	*V*	
	As	2.878	2.061	2.773	3.000		
(4, 4, 0)	P	2.213	1.789	1.932	2.254	*B*	√
	Sb	1.841	1.627	1.677	1.833		
	As	0.720	0.090	0.084	0.741		
(6, 6, 0)	P	0.472	0.082	0.068	0.582	*L*	√ ?
	Sb	0.370	0.076	0.062	0.425		
	As	0.682	···	0.270	0.777		
(10, 10, 0)	P	0.566	···	0.304	0.612	*M*	√ ?
	Sb	0.485	···	0.304	0.559		
	As	0.564	0.680	1.156	0.566		
(1, 1, 5)	P	0.474	0.587	0.784	0.524	*Q*	√
	Sb	0.433	0.533	0.675	0.387		
	As	0.332	0.841	1.394	0.242		
$(\bar{3}, \bar{3}, \bar{7})$	P	0.374	0.804	1.121	0.317	*X*	√ ?
	Sb	0.480	0.760	1.016	0.437		
	As	0.593	···	0.348	0.696		
$(\bar{3}, \bar{3}, \bar{11})$	P	0.502	···	0.344	0.662	*P*	
	Sb	0.417	···	0.331	0.629		
	As	1.608	0.872	1.517	1.292		
(5, 5, 1)	P	1.235	0.809	1.150	1.117	*D*	√ ?
	Sb	0.961	0.756	1.023	1.003		
	As	0.872	···	0.807	0.806		
(5, 5, 9)	P	0.777	···	0.781	0.764	*G*	√ ?
	Sb	0.706	···	0.747	0.761		
	As	0.719	···	1.037	0.718		
$(\bar{7}, \bar{7}, \bar{3})$	P	0.665	···	0.942	0.685	*I*	√ ?
	Sb	0.656	···	0.885	0.643		

TABLE VIII. (*Continued*).

Site	Donor	TGC[b]	Theory $a_l/2$ HM[c]	Present[d]	$a_l/2$	Experiment[a] Shell	Shell identified
	As	0.375	···	0.309	0.428		
(9,9,1)	P	0.344	···	0.323	0.379	*R*	√ ?
	Sb	0.318	···	0.316	0.332		

[a]Experimental values are for sites identified definitely (√) or tentatively (√ ?) or simply suggested (not identified) in Ref. 42.

[b]Second set of theoretical results by Castner, Ref. 42.

[c]Results due to Hale and Mieher, as given in Ref. 42.

[d]The following parameters are used: $k_i/k_{max} = 0.856$; $\eta = 178$; $a(\mathrm{As}) = 18.4$ a.u.; $a(\mathrm{P}) = 23.1$ a.u.; and $a(\mathrm{Sb}) = 25.0$ a.u.

[e]N. F. = not found.

points relative to the Δ_1 valleys.

Both the theoretical results by Hale and Mieher and those of the present calculations are based on the assumption that the donor wave function has components from only the six Δ_1 valleys of the conduction band. For all of the definitely identified sites, both theories give about the same agreement with experiment. However, it should be pointed out that the wave functions used by Hale and Mieher[49] are obtained by scaling the wave functions in the Kohn-Luttinger one-valley EMA.[1,2] Although there are no adjustable parameters in them, these wave functions do not give the observed ground-state energies. On the contrary, our calculated Fermi contact constants are actually predicted results from energy calculations. The wave functions are completely determined by the energies and contain no adjustable parameters.

VII. SUMMARY

A phenomenological two-parameter model impurity potential was proposed for shallow-level group-V donors in silicon. The multivalley effective-mass approximation was developed and used to calculate variationally the energy levels. The potential parameters were fitted to the observed $1s(A_1) \rightarrow 2p_\pm$ and $1s(T_2) \rightarrow 2p_\pm$ energies. It was shown that the proposed potential describes well the central-cell correction and the dielectric screening

It was found that for the p states, the usual one-valley effective-mass approximation is adequate. Also, in the multivalley EMA, the valley-orbit interaction shifts the $1s(A_1)$ level downward and the $1s(T_2)$ and $1s(E)$ levels upward relative to the one-valley-EMA $1s$ level.

The effects of the uncertainty in the position of the Δ_1 conduction-band valleys and of the coupling between the $1s$ and $2s$ states of the same symmetry on the ground-state energy and potential parameters were examined. These effects are small.

The contribution of the higher-energy subsidiary conduction-band minima to the ground-state energy was shown to be much smaller than that of the Δ_1 valleys.

Using the trial wave function of the ground state, the photo-ionization cross section was calculated. The spectral dependence of the photo-ionization cross section compares well with that given by Lucovsky's δ-function potential model and with experiment. The trial wave functions were also used to predict the Fermi contact hyperfine constants. The results give about the same agreement with ENDOR experiments as those previously reported.

ACKNOWLEDGMENT

The authors would like to acknowledge several helpful discussions with Professor J. Bardeen.

APPENDIX

In this Appendix we shall show that the impurity wave equation can be transformed into

$$[H^0 + U_\phi]\Phi = E\Phi \ , \tag{A1}$$

where

$$\Phi = \sum_{n\vec{k}} F_n(\vec{k})\psi^0_{nk} \tag{A2}$$

is the pseudo-wave-function, and ψ^0_{nk} is the Bloch function of the pure crystal satisfying

$$H^0\psi^0_{nk} = E^0_{nk}\psi^0_{nk} \ , \tag{A3}$$

and U_ϕ is the pseudo-impurity-potential.

We begin with the Schrödinger equations of the impure crystal, namely,

$$H\psi = [H^0 + U]\psi = E\psi \tag{A4}$$

and

$$H\psi_{\alpha'} = [H^0 + U]\psi_{\alpha'} = E_{\alpha'}\psi_{\alpha'} \ , \tag{A5}$$

where U is the true impurity potential, E and ψ are the energy and wave function of the valence state, and $E_{\alpha'}$ and $\psi_{\alpha'}$ are the energy and wave function of the core states. The core states are orthogonal to the valence states, so that

$$\langle \psi_{\alpha'} | \psi \rangle = 0 \ . \tag{A6}$$

To ensure that in solving the Schrödinger equation (A4) the energy obtained is E instead of $E_{\alpha'}$, we introduce the pseudo-wave-function Φ defined by

$$\psi = \Phi - \sum_{\alpha'} \langle \psi_{\alpha'} | \Phi \rangle \psi_{\alpha'} \ . \tag{A7}$$

Substituting (A7) into (A4), we find that Φ satisfies the equation

$$[H^0 + U + V_R]\Phi = E\Phi \ , \tag{A8}$$

where

$$V_R\Phi = \sum_{\alpha'} (E - E_{\alpha'}) \langle \psi_{\alpha'} | \Phi \rangle \psi_{\alpha'} \ . \tag{A9}$$

Since we are interested in impurity states of energy lying between the conduction and the valence bands, we may expand Φ in terms of the valence-state Bloch functions. Furthermore, since we consider H^0 as the unperturbed Hamiltonian and $U + V_R$ as the perturbation, we use the true Bloch functions for expansion. That is, we write

$$\Phi = \sum_{n\vec{k}} F_n(\vec{k}) \psi^0_{nk} \ . \tag{A10}$$

Putting (A10) into (A8), we obtain (A1), with

$$U_\phi \Phi = U\Phi + V_R\Phi \ . \tag{A11}$$

Some essential features of the pseudo-wave-equations (A1) and (A2) may be brought out in the Wannier-function representation. The Wannier functions of the pure crystal are defined by[50]

$$w^0_n(\vec{r} - \vec{R}_i) = (1/\sqrt{N}) \sum_{\vec{k}} \psi^0_{nk} e^{-i\vec{k}\cdot\vec{R}_i} \ . \tag{A12}$$

The inverse transform is

$$\psi^0_{nk} = (1/\sqrt{N}) \sum_i w^0_n(\vec{r} - \vec{R}_i) e^{i\vec{k}\cdot\vec{R}_i} \ . \tag{A13}$$

The core states of the pure crystal are thus

$$\psi^0_{\alpha k} = (1/\sqrt{N}) \sum_i w^0_\alpha(\vec{r} - \vec{R}_i) e^{i\vec{k}\cdot\vec{R}_i} \ , \tag{A14}$$

where, in the tight-binding approximation, $w^0_\alpha(\vec{r}_i - \vec{R}_i)$ looks just like the αth core orbital of a free silicon atom centered at R_i.[51] For simplicity, we consider a crystal with only one substitutional impurity. If we assume negligible overlap of the core orbitals centered at different lattice sites,[52] then the core states of the impure crystal, $\psi_{\alpha'}$, may be expanded as a linear combination of the Wannier functions, $w^0_\alpha(\vec{r} - \vec{R}_i)$, of the core band of the pure crystal plus a linear combination of the core orbitals of the isolated impurity atom, $\psi_{i\alpha'}(\vec{r})$. With this assumption and the orthogonality condition

$$\langle w^0_\alpha(\vec{r} - \vec{R}_i) | \psi^0_{nk} \rangle = 0 \ , \tag{A15}$$

Eqs. (A7) and (A9) become

$$\psi = \Phi - \sum_{\alpha'} \langle \psi_{i\alpha'} | \Phi \rangle \psi_{i\alpha'} \tag{A16}$$

and

$$V_R\Phi = \sum_{\alpha'} (E - E_{\alpha'}) \langle \psi_{i\alpha'} | \Phi \rangle \psi_{i\alpha'} \ , \tag{A17}$$

where the primed sums means only the core states of the impurity atom are summed. Thus, by expanding the pseudo-wave-function in terms of the valence-state true Bloch functions, the differences between the true and the pseudo-wave-functions and between the true and the pseudo-impurity-potentials vanish outside the impurity core region.

Hermanson and Phillips[53] chose to expand the pseudo-impurity-wave-functions in the pseudo-Bloch-functions of the pure crystal, i.e.,

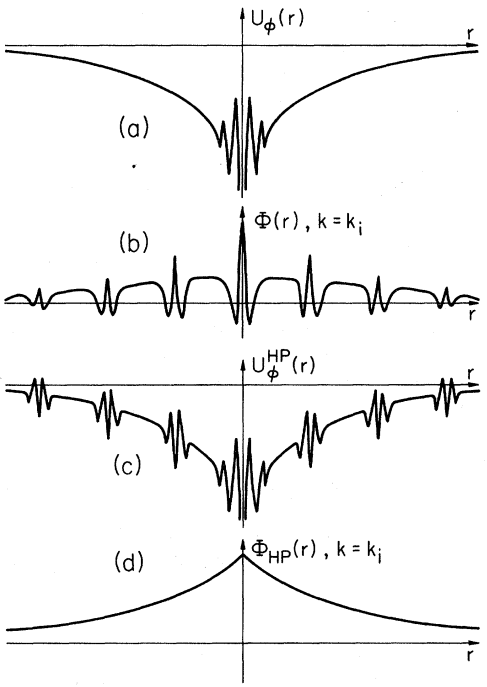

FIG. 7. Pseudo-impurity-wave-functions and potentials. In (a) and (b) the pseudo-wave-function is expanded in terms of the true Bloch functions. In (c) and (d) the pseudo-wave-function is expanded in terms of the pseudo-Bloch-functions.

$$\Phi_{HP} = \sum_{n\vec{k}} f_n(\vec{k}) \phi^0_{nk} \ . \tag{A18}$$

The pseudo-Bloch-function ϕ^0_{nk} is given by

$$\psi^0_{nk} = \phi^0_{nk} - \sum_\alpha \langle \psi^0_\alpha | \phi^0_{nk} \rangle \psi^0_\alpha \ , \tag{A19}$$

$$[H^0 + V^0_R]\phi^0_{nk} = E^0_{nk}\phi^0_{nk} \ , \tag{A20}$$

and

$$V^0_R\phi^0_{nk} = \sum_\alpha [E^0_{nk} - E^0_\alpha] \langle \psi^0_\alpha | \phi^0_{nk} \rangle \psi^0_\alpha \ , \tag{A21}$$

where ψ^0_α and E^0_α are the core-state wave function and energy of the pure crystal. The unperturbed Hamiltonian in this case is $[H^0 + V^0_R]$, so that the corresponding pseudo-impurity-potential is

$$U^{HP}_\phi\Phi = [U + V_R - V^0_R]\Phi \ . \tag{A22}$$

By using the fact that $\langle \psi^0_\alpha | \phi^0_{nk} \rangle \neq 0$, it can readily be seen that the differences $[\psi - \Phi_{HP}]$ and $[U^{HP}_\phi - U]$ are not localized within the impurity core region; instead, they oscillate in every core region of the crystal.

Actually, the two formalisms are equivalent. By expanding Φ in terms of the true Bloch functions, one works with a pseudo-wave-function and a pseudopotential which are the same as the true wave function and potential outside the impurity core region. There the difficulty lies in the eval-

uation of the matrix elements of the pseudo-impurity-potential between true Bloch states. On the other hand, by expanding Φ in terms of the pseudo-Bloch-functions, one is more justified using a plane-wave approximation for ϕ^0_{nk}. However, the difficulty in this case is how to take into account the oscillating pseudo-impurity-potential in each of the core regions of the crystal, as illustrated in Fig. 7(c). The differences in the pseudo-wavefunction and the pseudo-impurity-potential of the two methods are illustrated schematically in Figs. 7(a)–7(d). The effective-mass approximation is based on a smooth or slowly varying potential; and it is evident that U_ϕ in Fig. 7(a) is smooth except in the central cell, while U_ϕ^{HP} in Fig. 7(c) is not as smooth.

---

*Based in part on a doctoral thesis of T. H. Ning in Physics at the University of Illinois, 1971, which can be obtained from University Microfilms, Ann Arbor, Michigan. Work supported in part by the Advanced Research Projects Agency and the Air Force Office of Scientific Research.

†IBM Fellow.

[1]W. Kohn and J. M. Luttinger, Phys. Rev. 98, 915 (1955).

[2]W. Kohn, Solid State Phys. 5, 257 (1957).

[3]J. M. Luttinger and W. Kohn, Phys. Rev. 97, 869 (1955).

[4]R. L. Aggarwal and A. K. Ramdas, Phys. Rev. 140, A1246 (1965).

[5]G. Weinreich, J. Phys. Chem. Solids 8, 216 (1959).

[6]P. Csavinszky, J. Phys. Chem. Solids 24, 1003 (1963).

[7]A. M. K. Müller, Z. Naturforsch. 20a, 1476 (1965).

[8]A. Morita and H. Nara, J. Phys. Soc. Japan Suppl. 21, 234 (1966).

[9]M. Jaros, Phys. Status Solidi 36, 181 (1969).

[10]J. C. Phillips, Phys. Rev. B 1, 1540 (1970).

[11]A. Baldereschi, Phys. Rev. B 1, 4673 (1970).

[12]R. A. Faulkner, Phys. Rev. 184, 713 (1969).

[13]J. Appel, Phys. Rev. 133, A280 (1964).

[14]F. Herman and S. Skillman, *Atomic Structure Calculations* (Prentice-Hall, Englewood Cliffs, N. J., 1963).

[15]J. C. Slater, *Quantum Theory of Molecules and Solids* (McGraw-Hill, New York, 1965), Vol. 2, p. 276.

[16]W. A. Harrison, *Pseudopotentials in the Theory of Metals* (Benjamin, New York, 1966), p. 259.

[17]V. Heine, Solid State Phys. 24, 1 (1970).

[18]I. V. Abarenkov and V. Heine, Phil. Mag. 12, 529 (1965).

[19]A. O. E. Animalu and V. Heine, Phil. Mag. 12, 1249 (1965).

[20]J. C. Phillips, *Covalent Bonding in Crystals, Molecules, and Polymers* (University of Chicago Press, Chicago, 1969), Chap. 2.

[21]M. Jaros and P. Kostecky, J. Phys. Chem. Solids 30, 497 (1969).

[22]T. H. Ning and C. T. Sah, Solid State Commun. 8, 1893 (1970).

[23]H. Nara and A. Morita, J. Phys. Soc. Japan 21, 1852 (1966).

[24]M. Tinkham, *Group Theory and Quantum Mechanics* (McGraw-Hill, New York, 1964), p. 80.

[25]J. C. Hensel, H. Hasegawa, and M. Nakayama, Phys. Rev. 138, A225 (1965).

[26]C. D. Salberg and J. J. Villa, J. Opt. Soc. Am. 47, 244 (1957).

[27]M. Cardona, W. Paul, and H. Brooks, J. Phys. Chem. Solids 8, 204 (1959).

[28]A. Onton, Ph. D. thesis (Purdue University, 1967) (unpublished).

[29]W. E. Krag, W. H. Kleiner, and H. J. Zeiger, in *Proceedings of the Tenth International Conference on the Physics of Semiconductors* (U. S. Atomic Energy Commission, Division of Technical Information, Washington, D. C., 1970), p. 271.

[30]T. G. Castner, Phys. Rev. 155, 816 (1967).

[31]H. J. Hrostowski and R. H. Kaiser, J. Phys. Chem. Solids 7, 236 (1958).

[32]H. J. Hrostowski and R. H. Kaiser, J. Phys. Chem. Solids 4, 315 (1958).

[33]R. L. Aggarwal and A. K. Ramdas, Phys. Rev. 137, A620 (1965).

[34]See p. 104 of Ref. 15.

[35]L. Pauling, *The Nature of Chemical Bond*, 2nd ed. (Cornell U. P., Ithaca, N. Y., 1948), p. 343.

[36]J. T. Waber and D. T. Cromer, J. Chem. Phys. 42, 4116 (1965).

[37]G. Feher, J. Phys. Chem. Solids 8, 486 (1959).

[38]G. Feher, Phys. Rev. 114, 1219 (1959).

[39]E. B. Hale and T. G. Castner, Jr., Phys. Rev. B 1, 4763 (1970).

[40]M. L. Cohen and T. K. Bergstresser, Phys. Rev. 141, 789 (1966).

[41]E. O. Kane, Phys. Rev. 146, 558 (1966).

[42]T. G. Castner, Jr., Phys. Rev. B 2, 4911 (1970).

[43]T. G. Castner, Jr., E. B. Hale, and R. Craven, in Ref. 29, p. 613.

[44]M. Lax, in *Proceedings of the* 1954 *Atlantic City Conference on Photoconductivity* (Wiley, New York, 1956), p. 111.

[45]G. Lucovsky, Solid State Commun. 3, 299 (1965).

[46]E. Burnstein, G. Picus, and N. Sclar, in Ref. 44, p. 353.

[47]R. A. Messenger and J. S. Blakemore, Solid State Commun. 9, 319 (1971).

[48]A. Onton, Phys. Rev. Letters 22, 288 (1969).

[49]E. B. Hale and R. L. Mieher, Phys. Rev. 184, 751 (1969).

[50]J. M. Ziman, *Principles of the Theory of Solids* (Cambridge U. P., London, England, 1964), p. 149.

[51]Reference 50, p. 81.

[52]This assumption is not valid for the heavier impurities, such as Sb and Bi, where the d-shell electrons of the impurity cores may penetrate slightly into the neighboring cores.

[53]J. Hermanson and J. C. Phillips, Phys. Rev. 150, 652 (1966).